Anharmonic interactions of nonequilibrium phonons in $LiYF_4:Pr^{3+}$

Xiao-jun Wang, W. M. Dennis, and W. M. Yen
Department of Physics and Astronomy, University of Georgia, Athens, Georgia 30602
(Received 19 March 1992)

We have investigated the decay of nonequilibrium phonons in $LiYF_4:Pr^{3+}$ (1 at. %) at a temperature of 9.5 K. Nonequilibrium phonon populations at 51.9, 66.0, and 113 cm^{-1} are generated monochromatically with a high-power pulsed far-infrared laser via defect-induced one-phonon absorption, and their temporal and spectral evolution detected using anti-Stokes absorption. We observe the broadband distribution that results from the anharmonic decay of the initial monochromatic phonon population. The experimental data are modeled using a Monte Carlo simulation based on spontaneous three phonon processes. The simulation is in good agreement with the experimental data.

INTRODUCTION

Theoretical studies have shown that anharmonic interactions which involve three phonons dominate the relaxation of monochromatic high-frequency nonequilibrium phonons.[1-3] This prediction has been supported by a large body of experimental work.[4-6] However, due to the limitations of the techniques for high-frequency phonon generation and detection, the initial products from the decay of a monochromatic phonon distribution have not been previously observed. The phonon distributions which occur shortly after the generation of monochromatic phonons and before the onset of scaling behavior[3] provide additional information on the phonon decay processes. Broadband experiments that use heat pulse[7] or multiphonon absorption[8] for phonon generation, yield a convoluted distribution of phonon decay products thus limiting the frequency resolution. Monochromatic phonons created through electronic relaxation exhibit a strong resonant behavior. Additionally, the possibility of observing the initial decay products from such nonequilibrium phonons is also hindered by the low occupation number of the generated phonons. A narrow-band experiment was attempted in diamond by Schwartz and Renk.[9] However, the time resolution of their experiment (100 ns) was not sufficient to establish whether a monochromatic phonon population was generated or to detect the phonon decay products before several phonon generations had occurred.

In order to observe the initial broadband decay distribution it is therefore necessary to use a high occupation number monochromatic narrow-band source of bulk phonons combined with a highly sensitive frequency-selective detection. In this work, we use the combination of defect-induced one-phonon absorption (DIOPA) for phonon generation and an absorption vibronic sideband phonon spectrometer (AVSPS) for phonon detection. We present data on the temporal and spectral evolution of the nonequilibrium phonon distributions which result from monochromatic phonon generation in the Pr^{3+}-doped $LiYF_4$ (YLF) system.

We believe that, in addition to being the first study of high-frequency phonon dynamics in YLF that this is the first observation of the initial broadband distributions which directly result from the decay of a monochromatic phonon population. We point out that the phonon decay rates measured in this work are those for (1%) Pr^{3+}-doped YLF and that these rates are expected to be greater than those for the pure crystal. Investigations of anharmonic decay rates in $Ca_{1-x}Sr_xF_2$ mixed crystals[10] indicate that the phonon decay rates for a 1% impurity level are the order of a factor of 2 times greater than the pure crystal.

In many systems, high-frequency acoustic phonons are strongly scattered or trapped by the low-energy electronic transitions.[11,12] These processes can dominate the anharmonic interactions making them difficult to observe. In Pr^{3+}:YLF, there are no low-lying electronic levels in the frequency range of our investigation. The low phonon scattering rate combined with a comparatively high Debye frequency[13] thus makes this an ideal system to investigate purely anharmonic interactions.

In order to theoretically model the details of the broadband phonon evolution, we perform Monte Carlo (MC) simulations based on the isotropic, dispersionless, Debye long-wave approximation. The results of the simulation are in good agreement with the experimental data.

EXPERIMENT

The sample used in this experiment is 1 at. % and $2\times4\times6$ mm^3 Pr^{3+}-doped YLF crystal. A schematic of the phonon experimental setup used in this work is shown in Fig. 1. Nonequilibrium phonons are generated monochromatically using defect-induced one-phonon absorption of far-infrared (FIR) radiation from a superradiant cell pumped by a high-power transversely excited CO_2 laser. Phonon distributions are probed with both spectral and temporal resolution by monitoring the anti-Stokes absorption of a tunable dye laser. FIR pulse energies in excess of 6 mJ with pulse duration ~50 ns are obtained for the lines used in this experiment at frequencies of 51.9, 66.0, and 113 cm^{-1}. The frequency bandwidth of these pulses is less than 500 MHz as measured using a

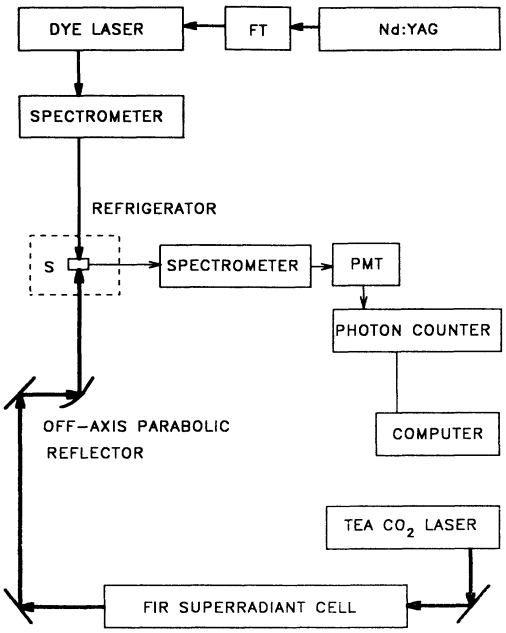

FIG. 1. A schematic of experimental setup. FT: frequency tripling crystal; S: sample.

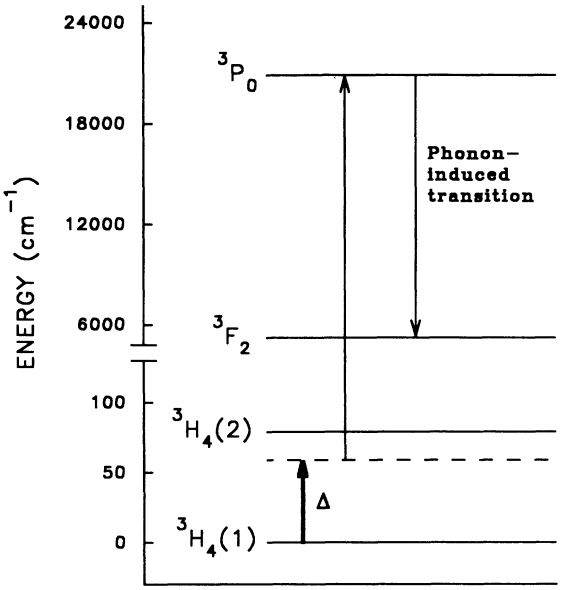

FIG. 2. Energy level diagram for Pr^{3+} in YLF. Nonequilibrium phonons of energy Δ are detected using AVSPS. Phonon-induced absorption is measured by monitoring the fluorescence from the $^3P_0 \rightarrow {}^3F_2$ transition.

FIR Fabry Perot interferometer. We estimate that greater than 30% of the initial FIR energy is incident on the sample with a 2-mm spot size. The FIR energy loss is due the gold reflectors used for beam steering and absorption in both the window of the cold head of refrigerator and the air in the FIR path. The optical detection pulses (0.6 mJ) are generated using a YAG pumped coumarin 480 dye laser in grazing incidence configuration. These pulses are then amplified and further spectrally filtered by a 1-m spectrometer. The timing of the experiment is controlled by a multi-channel delay-pulse generator, which is triggered by the flash lamp pulses from the Nd:YAG laser. Phonon transient signals are obtained by varying the pulse delay between the FIR and optical detection pulses via a dual gated photon counter. The phonon-induced fluorescence is detected using a RCA C31034A photomultiplier tube after spectral filtering using a 0.85-m double spectrometer. This detection scheme allows us to measure phonon temporal behavior in the range of 50 ns to 200 μs.

The phonon generation and detection pulses are incident on the sample in a colinear counter-propagating geometry. In the absence of phonons, an optical pulse with frequency Δ less than the $^3P_0$ zero-phonon line is transmitted through the sample without absorption. In the presence of phonons at the probe laser detuning Δ, anti-Stokes absorption to $^3P_0$ followed by fluorescence to $^3F_2$ occurs (Fig. 2). The time-integrated fluorescence is collected at 90° to both the generation and detection pulses, which provides a monitor of the evolution of nonequilibrium phonon population.

The sample is cooled to a temperature of 9.5 K using a two-stage closed-cycle refrigerator. Although the interactions between monochromatic and thermal phonons may contribute to phonon relaxation,[14,15] the results obtained in both Ref. 11 and this work suggest that these effects do not dominate at this temperature, i.e., we did not observe a significant nonequilibrium phonon population at $\Delta_{mon}+\Delta_{th}$, where Δ_{mon} and Δ_{th} are the frequencies of monochromatic and thermal phonons, respectively. An anti-Stokes calibration of the nonequilibrium phonon population can be obtained when the dye laser pulse is incident on the sample before the FIR pulse. The nonequilibrium occupation number at frequency Δ $n_{non}(\Delta,T)$, then can be calculated by

$$n_{non}(\Delta,T)=n_{th}(\Delta,T)\frac{\alpha(\varepsilon_0-\Delta)-\alpha_{th}(\varepsilon_0-\Delta)}{\alpha_{th}(\varepsilon_0-\Delta)} . \quad (1)$$

$n_{th}(\Delta,T)$ is the thermal occupation number at phonon energy Δ, which is given by the Bose-Einstein distribution. $\alpha(\varepsilon_0-\Delta)$ and $\alpha_{th}(\varepsilon_0-\Delta)$ are the phonon-induced absorption coefficients to the $^3P_0$ zero-phonon line at energy ε_0 in the presence of a nonequilibrium phonon population and a thermal phonon population, respectively. The absorption coefficients $\alpha_{th}(\varepsilon_0-\Delta)$ and $\alpha(\varepsilon_0-\Delta)$ are obtained from the total time-integrated phonon-induced fluorescence detected by the optical probe pulse before and after the FIR generation pulse, respectively. Arbitrary phonon numbers $N_{non}(\Delta,T)$ can be calculated from phonon occupation numbers by multiplying by Δ^2 according to the Debye approximation.

RESULTS AND DISCUSSION

Figure 3 shows the frequency dependence of phonon decay times. The open circles are measured with mono-

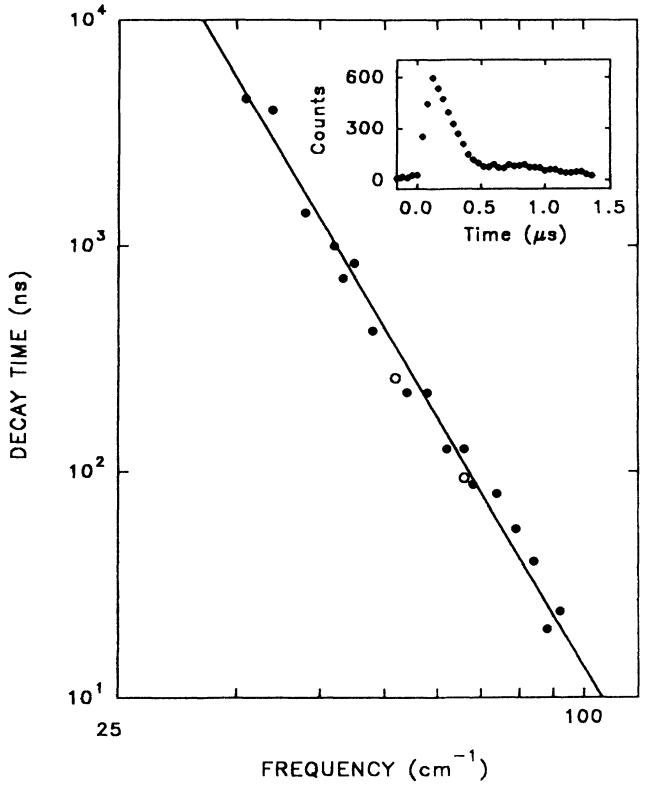

FIG. 3. Frequency dependence of the phonon decay time. The solid line represents the Δ^{-5} dependence expected from the isotropic dispersionless model. The open circles show the decay times of monochromatically generated phonons at 51.9 and 66.0 cm^{-1}. Solid circles show that of the decay products from a 113-cm^{-1} monochromatic phonon population.

chromatically generated phonons, i.e., $\Delta=\nu_g$, the FIR frequency. The solid circles are measured from the lifetimes of decay products of $\nu_g=113$-cm^{-1} phonons. The solid line represents the best fit to

$$\frac{1}{\tau_d}=A\Delta^5 , \tag{2}$$

where A is a constant and is a measure of the anharmonicity. This relationship is a direct consequence of the assumption that the system is an isotropic, dispersionless Debye crystal. The experimental value of A determined from Fig. 3 is 7.4×10^{-3} (cm^{-1})$^{-5}$s^{-1} for the YLF:Pr^{3+} system. The value of A for YLF:Pr^{3+} together with values for other materials[11,16] are provided for comparison in Table I. YLF:Pr^{3+} has a low value of A compared to other fluoride hosts, which is consistent with the result of low phonon decay rates observed in this system. The inset in Fig. 3 shows a typical phonon transient.

Phonon spectra are constructed from the phonon transients as described in Ref. 14. The spectral and temporal phonon evolution associated with the anharmonic decay of $\nu_g=66$-cm^{-1} phonons is shown in Fig. 4. The spectra are plotted in arbitrary phonon number, as this makes the symmetry associated with the anharmonic decay process more apparent. The monochromatic peak and a symmetric broadband spectral distribution centered at half the generation frequency can be seen at early times. The broadband distribution which occurs at early time is in a good agreement with $\Delta^2(\Delta_0-\Delta)^2$, the probability function for phonon decay from Δ_0 to Δ and $\Delta_0-\Delta$, where Δ_0 and $(\Delta,\Delta_0-\Delta)$ are, respectively, the frequencies of monochromatically generated phonons and a pair of daughter phonons. At late times, the maximum of the broadband distribution gradually downshifts in frequency due to further decay processes. The decay rate is different for all frequencies in the band according to the Δ^5 dependence.

Phonon dynamics is often described using a generation model.[17] Here, the phonon populations centered on Δ_0, $\Delta_0/2$, $\Delta_0/4$, etc., are treated as a series of Einstein modes.[17,18] A model of this nature obviously cannot describe the situation where phonons within a given band have different decay rates. In this work we compare our data to a Monte Carlo simulation. The simulation is based on the isotropic, dispersionless model and uses the result that

$$\frac{1}{\tau_d(\Delta)}\propto\int_0^{\Delta}\nu^2(\Delta-\nu)^2d\nu . \tag{3}$$

We note that the integral reduces to $1/\tau_d(\Delta)=A\Delta^5$ as expected. Δ can be any frequency between zero and Δ_0. Δ equals Δ_0 for the monochromatic phonon distribution and $\nu^2(\Delta_0-\nu)^2$ gives the profile of the initial phonon distribution. The Monte Carlo simulation is based on the following assumptions: (a) isotropic dispersionless Debye solid, (b) no phonon coalescence processes, (c) no stimu-

TABLE I. Comparison of A values for different crystals [in units of (cm^{-1})$^{-5}$s^{-1}].

Crystals	YLF:Pr^{3+}	LaF$_3$:Pr^{3+}	SrF$_2$:Pr^{3+}	CaF$_2$:Eu^{2+}	YAG:Pr^{3+}	Al$_2$O$_3$:Cr^{3+}
A (measured)	7.4×10^{-3}	4.3×10^{-1}[a]	8.1×10^{-2}[b]	1.2×10^{-3}[c]	1.3×10^{-3}[d]	1.22[b]
A (calculated)	1.4×10^{-4}[e]	2.6×10^{-1}[b]	3.7×10^{-1}[b]	1.4×10^{-1}[b]		1.1×10^{-2}[b]

[a]From Ref. 4.
[b]From Ref. 16.
[c]From Ref. 6.
[d]From Ref. 11.
[e]See Ref. 19.

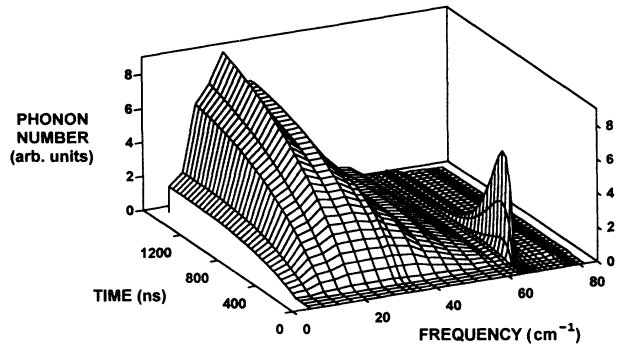

FIG. 4. Temporal and spectral evolution of monochromatic phonons generated at 66.0 cm^{-1}.

lated decay processes, (d) no monochromatic-thermal phonon interactions, and (e) phonons on all branches with same frequency have same decay rate due to rapid mode conversion.

A schematic of the MC simulation is shown in Fig. 5. The dashed line denotes an observation time t_0 for a range of decay products which result from different phonon generations and have different frequencies. This is a critical difference from the generation model where there is only one decay rate to next generation. The details of the simulation process may be summarized as follows.

(1) Only the first six generations are considered as this is more than sufficient to describe the phonon dynamics that occurs during the time scale of our experiment.

(2) The spectral and temporal resolution chosen for our simulation is 1 cm^{-1} and 4 ns, respectively.

(3) A phonon with energy Δ at any generation may break up into two phonons with any possible frequency combination of ν and $(\Delta-\nu)$ within the limitations of (2). The combination with the fastest decay rate is chosen to be the next generation.

(4) The decay rate for the initial monochromatic phonon population is determined experimentally and the rate to a given pair of daughter phonons calculated from a set of exponentially distributed pseudorandom number with a weighting function of $\nu^2(\Delta_0-\nu)^2$.

An alternate approach for steps (3) and (4) is to calcu-

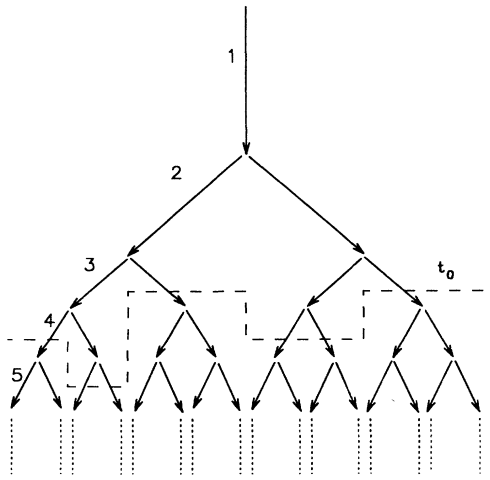

FIG. 5. Three-phonon process decay model of Monte Carlo simulation. t_0 represents a constant time.

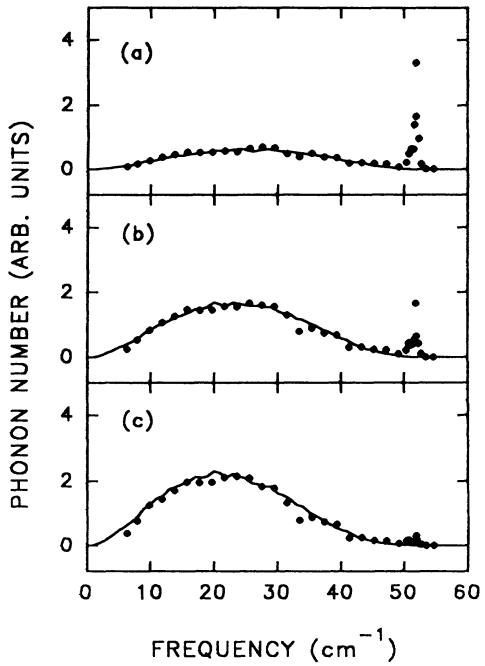

FIG. 6. Comparison of experimental data and Monte Carlo simulation for the decay products of 51.9-cm^{-1} monochromatic phonons. (a) $t_0=40$ ns, (b) $t_0=400$ ns, (c) $t_0=800$ ns.

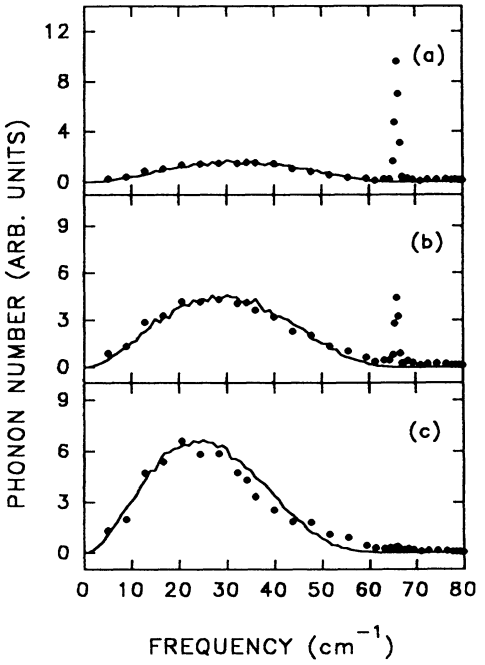

FIG. 7. Comparison of experimental data and Monte Carlo simulation for the decay products of 66.0-cm^{-1} monochromatic phonons. (a) $t_0=40$ ns, (b) $t_0=280$ ns, (c) $t_0=480$ ns.

late the decay rate for a phonon with energy Δ based on the Δ^5 dependence, and then assign the frequencies of the daughter phonons $(\nu, \Delta-\nu)$ using a set of random numbers distributed according to $\nu^2(\Delta-\nu)^2$. Identical results were obtained from both simulations. Figure 6 shows the comparison of experimental data and simulational results for the spectral distributions respectively at 40, 400, and 800 ns after the monochromatic generation at 51.9 cm^{-1} with 10^6 initial phonons. There is only one adjustable parameter to fit all the traces and that is the peak of the initial phonon distribution. The initial phonon lifetime of 250 ns is obtained from the resonant decay shown in Fig. 3. No attempt was made to model the details of the far-infrared pumping of the initial monochromatic phonon population.

Considering the simplicity of the model, we believe the agreement shown in Fig. 6 is excellent. The comparison for 66-cm^{-1} phonon generation is also shown in Fig. 7 with spectral distribution at 40, 280, and 480-ns delay. The initial decay time of 100 ns for simulation is measured from the resonant transient. Again, with only one adjustable parameter, we observe good agreement between simulations and experimental data although a deviation from the simulation appears for high phonon frequencies at late times. We attribute this feature to broadband backfeeding of the major peak at 25 cm^{-1}. The resonant transient at 66 cm^{-1} exhibits a nonexponential tail due to this effect. The addition of these processes to our model is the subject of a continuing investigation.

CONCLUSIONS

We have performed an investigation of the relaxation of high-frequency phonons in YLF:Pr^{3+}. We observe the initial phonon distributions which arise as a result of a three-phonon spontaneous decay of a monochromatic phonon population. We have compared our experimental results with a Monte Carlo simulation based upon the isotropic dispersionless model and obtain good agreement between experimental and simulation.

ACKNOWLEDGMENTS

The authors wish to thank D. S. Hamilton and A. M. Ferrenberg for useful discussions. This work was supported by National Science Foundation Grant Nos. DMR 8717696 and DMR 9015468.

[1]R. Orbach and L. A. Vredevoe, Physics **1**, 91 (1964).
[2]G. Klemens, J. Appl. Phys. **38**, 4573 (1967).
[3]Y. B. Levenson, in *Nonequilibrium Phonons in Nonmetallic Crystals,* edited by W. Eisenmenger and A. A. Kaplyanskii (North-Holland, Amsterdam, 1986), Chap. 3.
[4]W. A. Tolbert, W. M. Dennis, and W. M. Yen, Phys. Rev. Lett. **65**, 607 (1990).
[5]R. S. Meltzer, J. E. Rives, and G. S. Dixon, Phys. Rev. B **28**, 4786 (1983).
[6]R. Baumgartner, M. Engelhardt, and K. F. Renk, Phys. Rev. Lett. **47**, 1403 (1981).
[7]W. E. Bron and W. Grill, Phys. Rev. B **16**, 5303 (1977).
[8]U. Happek, R. Baumgartner, and K. F. Renk, in *Phonon Scattering in Condensed Matter,* edited by W. Eisenmenger, K. Lassmann, and S. Döttinger (Springer-Verlag, Berlin, 1984), Vol. 37.
[9]H. Schwartz and K. F. Renk, Solid State Commun. **54**, 925 (1985).
[10]U. Happek, W. W. Fischer, and K. F. Renk, in *Proceedings of the Third International Conference of Phonon Physics,* edited by S. Hunklinger, W. Ludwig, and G. Weiss (World Scientific, Singapore, 1990), p. 1248.
[11]Xiao-jun Wang, J. Ganem, W. M. Dennis, and W. M. Yen, Phys. Rev. **44**, 900 (1991).
[12]S. S. Yom, R. S. Meltzer, and J. E. Rives, Phys. Rev. B **36**, 6664 (1987).
[13]P. Blanchfield and G. A. Saunders, J. Phys. C **12**, 4673 (1979).
[14]Xiao-jun Wang, W. M. Dennis, and W. M. Yen, Phys. Rev. Lett. **67**, 2807 (1991).
[15]C. Herring, Phys. Rev. **95**, 954 (1954).
[16]W. E. Bron, Phys. Rev. B **21**, 2627 (1980).
[17]W. L. Schaich, Solid State Commun. **49**, 55 (1984).
[18]T. E. Wilson, F. M. Lurie, and W. E. Bron, Phys. Rev. B **30**, 6103 (1984).
[19]Calculated from Eq. (3) in Ref. 1 with a canonical value of 10^{11} N/m^2 for C_1, C_2, C_4, and C_5. Acoustic phonon velocity $v_l = 5.58 \times 10^3$ and $v_t = 1.85 \times 10^3$ m/s are used from Ref. 12. Mass density $\rho = 4 \times 10^3$ kg/m^3.